**Article:**
Zhang, H, He, X, Hua, Y et al. (2021) Corrosion behaviors of carbon steel induced by life activities of Phaeodactylum tricornutum in a marine environment. Materials and Corrosion, 72 (6). pp. 1065-1075. ISSN: 0947-5117

https://doi.org/10.1002/maco.202012183

**Article type:** Article

# Corrosion behaviors of carbon steel induced by life activities of *Phaeodactylum tricornutum* in a marine environment

Han Zhang [1,2], Xiaoyan He [1,2,3], Yong Hua [3], Xiuqin Bai [1,2], Chengqing Yuan [1,2]

[1] Reliability Engineering Institute, National Engineering Research Center for Water Transport Safety, Wuhan University of Technology, Wuhan 430063, China

[2] Key Laboratory of Marine Power Engineering and Technology, Ministry of Transport, Wuhan University of Technology, Wuhan 430063, China

[3] Institute of Functional Surfaces, School of Mechanical Engineering, University of Leeds, Leeds LS2 9JT, United Kingdom

Correspondence: Xiuqin Bai, Reliability Engineering Institute, National Engineering Research Center for Water Transport Safety, Wuhan University of Technology, Wuhan 430063, China

Email: xqbai@whut.edu.cn

Abstract

Microbiologically influenced corrosion (MIC) induced by bacteria has been studied for many years. Corrosion is known to be sensitive to the presence of microalgae, such as *Phaeodactylum tricornutum*. However, the life activity of the *P. tricornutum* that influences the general and localized corrosion of carbon steel is not fully understood. The current study used a combination of immersion tests and electrochemical experiments with a detailed surface characterization to reveal the naturally formed corrosion products with/without the presence of *P. tricornutum*. The results show that samples suffer from pitting corrosion and the averaged pit depths are approximately 15 μm under normal conditions of the light-dark

cycle or in a 24h-constant light condition. Meanwhile, the corrosion products are mainly comprised of γ-FeOOH and $Fe_3O_4$ in a constant light condition but γ-FeOOH, $Fe_3O_4$ and $FeCO_3$ were found in a light-dark cycle. This study proposed the fundamental mechanisms of the effect of *P. tricornutum* life activities on the corrosion performance of Q235 carbon steel, to fulfill the knowledge gaps of the presence of microalgae induce the general and pitting corrosion of carbon steel.

Keywords: carbon steel; corrosion morphology; electrochemical; microbiologically influenced corrosion

## 1 INTRODUCTION

Corrosion, one of the common metallic failure, has caused huge economic loss all over the world [1-3]. The complex marine environment exacerbates the metal corrosion due to the presence of high concentrate salt and various biological bacteria. With regards to the application of marine equipment and shipbuilding, steel components, especially Q235 carbon steel, are a common material option based on its good mechanical performance and relatively low price [4]. However, Q235 steel is prone to subject to corrosion in marine environments since the presence of various biological bacteria, leading to microbiologically influenced corrosion (MIC) on the surface [5].

There were many research efforts on MIC in marine environments [6, 7], such as microorganisms including bacteria, fungi and algae [8, 9]. The study of MIC caused by bacteria has been widely studied in the literature, these studies largely focused on the corrosion behaviors of carbon steel in sulfate reducing bacteria (SRB)-containing suspension [10, 11]. Sun et al [12] pointed out that the corrosion rate of Q235 with SRB was higher than that without SRB. They found that the cathodic current density of steel immersed in the soil

with SRB was larger than that without SRB. Yue et al [13] found that the iron-oxidizing bacteria (IOB) increased the corrosion damage of the steel and pits were observed on the steel surface. Several MIC theories are relative to bacteria have been proposed, such as cathodic depolarization theory [14, 15], biopolymer-induced corrosion theory [16], local corrosive cell theory [17]. The presence of algae in the biofouling process is also responsible for MIC [18].

A summary of investigations into the effect of algae on the corrosion behaviors of carbon steel was conducted. Allwright et al. [19] found that corrosion of carbon steel immersed in the seawater with the presence of algae is severer than that of the removal of algae. Liu et al. [18] found that the averaged corrosion rate of carbon steel in *Chlorella vulgaris*-containing suspension was approximately 4 times higher than that of without *Chlorella vulgaris*, suggesting that the large corrosion rates were owing to the damage of iron phosphate film and crevice corrosion [18]. These studies largely concentrated on the presence of algae accelerating the corrosion processes at the material interface [20], with very little focus on the corrosion behavior of carbon steel regarding the algal life activities, such that *Phaeodactylum tricornutum* (*P. tricornutum*), a type of widespread marine algae. As an autotrophic organism, *P. tricornutum* shows photosynthesis in the light and respiration process in the dark, prone to form biofilm in a marine environment [21].

The current study focuses on the understanding of corrosion behaviors of carbon steel due to the life activities of *P. tricornutum* in a marine environment. In this study, Q235 carbon steel samples were incubated in *P. tricornutum* suspensions at various light-dark cycles for 7 days. The influence of photosynthesis in the light cycles and respiration process in the dark cycles of *P. tricornutum* on the corrosion behaviors of Q235 carbon steel were investigated to reveal the corrosion mechanisms. The study provides a full comparison between the general

corrosion and localized corrosion in a marine environment, highlighting the importance of localized corrosion measurements due to the algal life activities.

## 2 Experimental procedures

### 2.1 Material sample preparation

Q235 carbon steel (C 0.3%, Si 0.01%, Mn 0.42%, S 0.029%, P 0.01%, Fe balance) were chosen as the experiment materials. The specimens with a diameter of 10 mm were used for the corrosion experiment. The electrochemistry samples were embedded within an epoxy resin, leaving one surface area of 0.785 $cm^2$ exposed to a 120 mL solution. The sample preparation process includes wet-polishing the surface with 400, 600, 1000 and 1200-grit silicon carbide paper, followed by acetone, 99% ethanol and distilled water and subsequently dried in a vacuum oven. To prevent the influence of other microorganisms, these samples were sterilized with UV light for 30 minutes before experiments [22]. The prepared samples were immediately used in both electrochemistry and immersion experiments.

### 2.2 Microbiological cultivation

The Artificial Sea Water (ASW) was contained ($g \cdot L^{-1}$) NaCl 24.53; $MgCl_2$ 5.20; $Na_2SO_4$ 4.09; $CaCl_2$ 1.16; $NaHCO_3$ 0.201; KBr 0.101; $H_3BO_3$ 0.027; $SrCl_2$ 0.025; NaF 0.003 with a pH value of 8.2 in accordance with ASTM Standard D1141-98 [23]. *P. tricornutum* was cultured in sterilized silicate-enriched Guillard F/2 growth medium. To ensure a sterile environment, the transfer of *P. tricornutum* was carried out in a sterile cabinet and then *P. tricornutum* was incubated in an illumination incubator (GZP-250S, Shanghai Jinghong experimental equipment co. ltd) at 20 ℃.

### 2.3 Weight loss measurement

The immersion tests were conducted immediately after sample preparation. A high-precision analytical balance (METTLER TOLEDO-MS1040TS/02, 0.1 mg) was used to measure the weight loss of samples before and after the immersion experiments. To study the role of *P. tricornutum* life activities on the corrosion behaviors of carbon steel, three sets of tests were performed, and carbon steel samples were immersed in sterile ASW as a comparison. The intensity of the light is 3000lux within the illumination incubator. The experimental conditions are provided in Table 1, the concentration of dissolved oxygen was measured by a dissolved oxygen meter (METTLER TOLEDO Seven Go (Duo) Pro) and pH values were detected at the same time.

After the test, the samples were taken out from the vessel and weight again. Samples were placed in a beaker containing deionized water, ultrasonically shaken for 1 minute in order to remove the unadhered biofilm layer. A chemically cleaning in order to remove the corrosion products on the surface was performed in Clarke's solution (20g antimony trioxide + 50g stannous chloride + 1000 mL 38% hydrochloric acid) according to ASTM Standard G1-03 [24, 25], followed by deionized water and dried in a vacuum oven. The corrosion rate (mm·a$^{-1}$) was calculated using equation (1):

$$V_{corr} = \frac{8.76 \times 10^4 \, \Delta m}{A t \rho} \quad (1)$$

where $V_{corr}$, $\Delta m$, $\rho$, $A$ and t were corrosion rate (mm·y$^{-1}$), weight loss (g), density (g·cm$^{-3}$) and area of specimens (cm$^2$), culture time (h), respectively.

### 2.4 Electrochemical measurements

A standard three-electrode cell was used for the electrochemical tests. Q235 carbon steel was used as the working electrode, a 1 × 1 cm$^2$ platinum plate as the counter electrode and a

Saturated Calomel Electrode (SCE) was used as the reference electrode. All the electrochemistry measurements were carried out at a steady Open Circuit Potential (OCP). The Electrochemical Impedance Spectroscopy (EIS) measurements were conducted in the frequency ranges from $10^2$ kHz to 10 mHz via an amplitude of 10 mV and the EIS result was fitted by ZVIEW software. The Tafel plots were performed in the potential ranged from -300 mV to 300 mV versus OCP with a scan rate of 0.5 mV· $s^{-1}$.

### 2.5 Surface and component analysis

After the immersion tests, the samples were washed with sterile ASW to remove unadhered algae and place in a 2.5% glutaraldehyde for 8 h at 4°C. Scanning electron microscopy (SEM, TESCAN VEGA3) was used to characterize the morphologies of corrosion products and biofilm formed on the surface. The X-ray Diffraction (D8 Advance) and Energy Dispersive Spectrometer (EDS, X-stream2 SDD, OXFORD Instrument Ltd.) were used to identify the nature of the corrosion products formed on the surface in an ASW containing *P. tricornutum* at various light-dark cycles. After the removal of corrosion products, 3D Laser scanning confocal microscope (Keyence, VK-X 1000 series) was used to measure the localized corrosion.

## 3 RESULTS

### 3.1 The identification of dissolved oxygen and pH in algal suspension

The concentration of dissolved oxygen and pH values in an ASW with the presence of *P. tricornutum* at various cycle conditions are provided in Figure 1. The measured oxygen in an ASW is maintained stable at the ranges of 7.5~8.5 mg·$L^{-1}$ with times, however, it can be noted that the presence of *P. tricornutum* causes variations of both oxygen and pH measurements. In

the 24 h-constant light cycles, the dissolved oxygen maintains at a higher level, fluctuating between 9.8 and 11.0 $mg \cdot L^{-1}$ within the whole 7 days of exposure time compared with 24 h-constant dark cycles, the dissolved oxygen is 5.0~6.0 $mg \cdot L^{-1}$. As for the light-dark cycles for 7 days, it is interested to note that the dissolved oxygen increases in light times, but low levels of dissolved oxygen were found in the dark times as expected.

A similar trend was measured for the pH curves as shown in Figure 1b. In the 24 h-constant light cycles for 7 days, the *P. tricornutum* consumes $CO_2$ via the process of photosynthesis, resulting in an increase of solution pH and the dissolved oxygen concentration. In the 24 h-constant dark cycles for 7 days, $CO_2$ is produced due to the process of respiration, consuming oxygen level from the solution and the decrease in solution pH was observed. The results suggest that the active *P. tricornutum* plays an important role in the corrosion process of carbon steel due to the variation of the dissolved oxygen levels, concentration of $CO_2$ and pH values, more detailed corrosion measurements are discussed in the following paragraphs.

### 3.2 Electrochemical measurements

Figure 2 shows the OCP curves of carbon steel samples exposed to the ASW with/without the presence of *P. tricornutum* suspension under various cycles for 7 days. High OCP values were recorded in the early stage and dropped significantly within 24 h for all the conditions. It is noted that the light affects the life activity of *P. tricornutum* that a positive shift was observed during the constant light cycles, the results coincide with Marconnet et al., who suggests that the presence of *P. tricornutum* change the local physiochemistry state through the production of oxygen to the increased OCP under the constant light [8].

The Tafel plots of samples exposed to ASW under various life activities of *P. tricornutum* after 7 days of exposure are provided in Figure 3. The polarization curves shift to the positive directions under the light-dark cycles and 24 h-constant light cycles, while it shifts to the negative direction in the 24 h-constant dark cycles after 7 days, suggesting that the positive shift of corrosion potential ($E_{corr}$) is contributed to the increase in the dissolved oxygen concentration, which is related to the photosynthesis of *P. tricornutum*.

The fitted electrochemical parameters are listed in Table 2. The smallest current density ($I_{corr}$) was observed for the 24 h-constant dark cycles. After the overall 7 days of exposure, the levels of corrosion rates follow the trend of 24 h-constant dark cycles > 24 h-constant light cycles > light-dark cycles > ASW under the current test conditions.

The Nyquist and Bode plots of samples at different cycle conditions after 1, 4 and 7 days of exposure are shown in Figure 4. After the first 24 hours, the semicircles of all the conditions are similar (Figure 4a), suggesting that the corrosion resistance of carbon steels has no significant difference in the early stage. After 4 days of exposure, an obvious decrease in the capacitive arc radius was found, especially in the condition of the constant light cycle (Figure 4c and e). There are two sub-peaks in the bode diagram in Figure 4b. The peak in the low-frequency region comes from the electric double layer and the peak in the high-frequency region comes from the corrosion product films. The peaks in the bode diagram become more obvious with times (Figure 4d and f), which suggests that the mixed film was covered the entire surface. Meanwhile, the diameters of semicircle decrease with immersion times, suggesting the presence of *P. tricornutum* accelerates the corrosion processes in both 24 h-constant light cycle and 24 h-constant dark cycle cases.

The EIS curves are fitted to equivalent circuit models and the fitted data is summarised in Table S1. The one-time constant and two-time constant electrical equivalent circuits are shown in Figure 5. $R_{ct}$ represents a charge transfer resistance and $Q_{dl}$ represents a double layer capacitance. In the two-time constant model, $R_f$ and $Q_f$ represent resistance and a capacitance of the mixed film, respectively.

### 3.3 Immersion test

The surface morphologies of samples after the removal of corrosion products are shown in Figure 6 and Figure S1. For all the conditions, the localized corrosion rates are higher than the general corrosion rates. The results indicate that the life activities of *P. tricornutum* accelerate the corrosion behavior of Q235 carbon steel. The general corrosion rates of 0.14 $mm \cdot a^{-1}$ under 24 h-constant dark cycle, 0.11 $mm \cdot a^{-1}$ under 24 h-constant light cycle and 0.08 $mm \cdot a^{-1}$ under light-dark cycle were recorded after 7 days of exposure respectively. It can be seen that the samples were exposed to the condition of 24 h-constant dark cycle after 7 days indicating the highest localized corrosion rate (Figure 6f). In a 24 h-constant light cycle for 7 days, the pit diameters are larger and more than 2 times deeper than that in the condition of the light-dark cycle. Figure 1S presents the recorded localized corrosion morphologies varied as a function times, indicating that the localized corrosion rates become severe with times for all the conditions. The results suggest that the localized corrosion measurements represent the real threat for samples immersed in ASW with/without the presence of algal suspension. The $O_2$ production via photosynthesis enhanced the localized corrosion.

### 3.4 Surface characterizations

Figure 7 and S2 represent the surface morphology of the microbial adhesion and the growth of the corrosion products on the surface at various immersion times and cycle conditions via

SEM. The life activities of *P. tricornutum* influence the surface morphologies of samples (Figure 7). It can be noted that the loose and porous corrosion products are formed on the surface of carbon steel samples immersed in ASW for the 1st, 3rd, 5th, and 7th day (Figure S2a and Figure 7a). The EDS results show that the corrosion products are rich in Fe, O and Cl, suggesting that the product could be iron oxide or hydroxide.

For the samples immersed in the *P. tricornutum* suspension, both corrosion products and *P. tricornutum* were observed on the sample surface (Figure 7b-d). The corrosion products are porous, larger gaps and holes were observed compared to that of the corrosion products observed in ASW as shown in Figure 7a, suggesting that the life activities of *P. tricornutum* change the corrosion product morphology via the photosynthesis $O_2$ production at light times and carbonic acid production due to respiration at dark times. The observed C and O via EDS indicate that the presence of *P. tricornutum* participates in the corrosion process. Elements of Mg, P, N, Si were detected within the corrosion products, which could be from the complexation of extracellular polymeric substance (EPS) and *P. tricornutum* [18].

To identify the formation of the corrosion products at various cycle conditions, the corrosion products were characterized by XRD (Figure 8). Lepidocrocite (γ-FeOOH) and magnetite ($Fe_3O_4$) are found in ASW and 24 h-constant light cycles after 7 days of exposure. In 24 h-constant dark cycles for 7 days, the corrosion products were detected mainly as siderite ($FeCO_3$). In light-dark cycles for 7 days, the corrosion products are comprised of γ-FeOOH, $Fe_3O_4$ and $FeCO_3$. The results suggest that the release of $CO_2$ via the respiration activity of *P. tricornutum* at night, leading to consuming the $O_2$ within the solution, consequently the formation of $FeCO_3$ crystals on the surface.

## 4 DISCUSSION

A proposed mechanism of the presence of *P. tricornutum* induces pitting corrosion was discussed (Figure 9). Under the 24 h-constant light cycles, both anodic and cathodic processes are accelerated by the produced oxygen from the photosynthesis of *P. tricornutum*. The anodic dissolution of $Fe^{2+}$ and the cathodic reaction is beginning with the depolarization of oxygen [26]:

$$Fe - 2e^- \rightarrow Fe^{2+} \quad (2)$$

$$O_2 + 2H_2O + 4e^- \rightarrow 4OH^- \quad (3)$$

The production of $OH^-$ continues to react with $Fe^{2+}$ to form Fe $(OH)_2$ on the surface which acts as a diffusion barrier, reducing the corrosion process via inhibiting the corrosive species pass through the layer. The intermediate corrosion product Fe $(OH)_2$ continues to form FeOOH and $Fe_3O_4$ via the following reactions [27, 28]:

$$2Fe^{2+} + O_2 + 2H_2O + 2e^- \rightarrow 2Fe(OH)_2 \quad (4)$$

$$2Fe(OH)_2 + 1/2O_2 \rightarrow 2FeOOH + H_2O \quad (5)$$

$$FeOOH + e^- \rightarrow Fe_3O_4 + H_2O \quad (6)$$

At the anodic site, Fe loses electrons to form $Fe^{2+}$ and continues oxidizing into Fe(III) (FeOOH, $Fe_3O_4$), which is confirmed by XRD, the surface covered with corrosion products becomes the cathode, the uncover region has a high dissolution rate compared to the covered region, leading to the formation of pits on the surface of the sample. The loose and porous corrosion products facilitated the diffusion of $Cl^-$, resulting in severer pitting corrosion. Therefore, obvious pitting corrosion was observed in the samples in algal suspension in the condition of a constant light cycle (Figure 6).

Under the constant dark cycle, the presence of *P. tricornutum* consumes oxygen through respiration to produce $CO_2$ which reacts with water to form $H_2CO_3$ and $HCO_3^-$ [29-31].

$$CO_{2(g)} \rightarrow CO_{2(aq)} \quad (7)$$

$$CO_{2(aq)} + H_2O \rightarrow H_2CO_{3(sol)} \quad (8)$$

$$2H_2CO_3 + 2e^- \rightarrow H_2 + 2HCO_3^- \quad (9)$$

$$2HCO_3^- + 2e^- \rightarrow H_2 + 2CO_3^{2-} \quad (10)$$

The anodic reaction of carbon steel in an aqueous $CO_2$ solution is primarily the dissolution of Fe [29, 31] :

$$Fe \rightarrow Fe^{2+} + 2e^- \quad (11)$$

The XRD results indicate that a large amount of $FeCO_3$ was formed on the surface in the algal suspension under the 24 h-constant dark cycle after 7 days. The driving force for the growth of $FeCO_3$ is relative to the supersaturation ratio (S).

$$S_{FeCO_3} = \frac{C_{Fe^{2+}} . C_{CO_3^{2-}}}{K_{SP}} \quad (12)$$

Where $C_{Fe^{2+}}$ and $C_{CO_3^{2-}}$ are the concentrations of $Fe^{2+}$ and $CO_3^{2-}$, respectively and $K_{SP}$ is the solubility of $FeCO_3$. The precipitate of the crystalline $FeCO_3$ once the concentration of $C_{Fe^{2+}}$ and $C_{CO_3^{2-}}$ ions exceed the solubility limit [29]. $FeCO_3$ precipitates on the surface of steel according to the following reaction:

$$Fe^{2+} + CO_3^{2-} \rightarrow FeCO_3 \quad (13)$$

In the light-dark cycle after 7 days, the formation of γ-FeOOH, $Fe_3O_4$ due to the presence of $O_2$ production via photosynthesis, and the growth of $FeCO_3$ crystals in a $CO_2$ containing media suggests that a large amount of $CO_2$ was produced during the respiration at dark time. Furthermore, the production of extracellular EPS by *P. tricornutum* has a strong complexation ability for metal cations (Figure 7), such as the consumption of $Fe^{2+}$ ions via the secretion of EPS to accelerate the dissolution of $Fe^{2+}$ and increases corrosion rate [5, 32].

## 5 CONCLUSIONS

The presence of *P. tricornutum* adsorbs to the surface of carbon steel and induces the MIC. The general corrosion rate of carbon steel with the presence of *P. tricornutum* is 3.5 times higher than that of the absence of *P. tricornutum*. The life activities of *P. tricornutum* has influences on the corrosion behavior of Q235 carbon steel. After 24 h-constant light cycle for 7 days, photosynthesis of *P. tricornutum* increases the local oxygen concentration to inducing pitting corrosion. The porous corrosion products are mainly comprised of γ-FeOOH and $Fe_3O_4$. In 24 h-constant dark cycle for 7 days, the production of $CO_2$ by aspiration enhances the formation of crystalline $FeCO_3$ on the surface which provides better corrosion protection to the surface compared with γ-FeOOH and $Fe_3O_4$. In the case of light-dark cycle after 7 days, both general and localized corrosion occurs and the corrosion products are mainly γ-FeOOH, $Fe_3O_4$ and $FeCO_3$.

## ACKNOWLEDGEMENTS

This work was supported by the National Natural Science Foundation of China (Grant No. 52071246 and 52001238), and International Postdoctoral Exchange Fellowship Program (Grant No. 20190060).

## AUTHOR CONTRIBUTIONS

**Han Zhang:** Investigation, Methodology, Data curation, Formal analysis, Writing - original draft, Writing - review & editing. **Xiaoyan He:** Data curation, Supervision, Writing - review & editing. **Yong Hua:** Supervision, Writing - review & editing. **Xiuqin Bai:** Supervision, Writing - review & editing. **Chengqing Yuan:** Supervision, Writing - review & editing.

## CONFLICT OF INTEREST

The authors declare no financial or commercial conflict of interest.

## DATA AVAILABILITY STATEMENT

Statement for Data available on request from the authors: The data that support the findings of this study are available from the corresponding author upon reasonable request.

## REFERENCES


[1] X. He, Y. Liu, J. Huang, X. Chen, K. Ren, H. Li, *Appl. Surf. Sci.* **2015**, 332, 89.

[2] L. Abdoli, J. Huang, H. Li, *Mater. Chem. Phys.* **2016**, 173, 62.

[3] P. Bai, H. Zhao, S. Zheng, C. Chen, *Corros. Sci.* **2015**, 93, 109.

[4] C. Du, X. He, F. Tian, X. Bai, C. Yuan, *Coatings* **2019**, 9, 398.

[5] F. Tian, X. He, X. Bai, C. Yuan, *Int. Biodeter. Biodegr.* **2020**, 147, 104872.

[6] S. Maruthamuthu, B.D. Kumar, S. Ramachandran, B. Anandkumar, S. Palanichamy, M. Chandrasekaran, P. Subramanian, N. Palaniswamy, *Ind. Eng. Chem. Res.* **2011**, 50, 8006.

[7] X. He, Y. Liu, Y. Gong, C. Zhou, H. Li, *Surf. Coat. Technol.* **2017**, 309, 295.

[8] C. Marconnet, C. Dagbert, M. Roy, D. Féron, *Corros. Sci.* **2008**, 50, 2342.

[9] N.O. San, H. Nazir, G. Donmez, *Corros. Sci.* **2011**, 53, 2216.

[10] S. Chen, P. Wang, D. Zhang, *Corros. Sci.* **2014**, 87, 407.

[11] J. Łabanowski, T. Rzychoń, W. Simka, J. Michalska, *Mater. Corros.* **2019**, 70, 1667.

[12] C. Sun, J. Xu, F. Wang, C. K. Yu, *Mater. Corros.* **2010**, 61,762.

[13] Y. Yue, M. Lv, M. Du, *Mater. Corros.* **2019**, 70, 1852.

[14] P. Zhang, D. Xu, Y. Li, K. Yang, T. Gu, *Bioelectrochemistry* **2015**, 101, 14.

[15] L. Lv, S. Yuan, Y. Zheng, B. Liang, S.O. Pehkonen, *Ind. Eng. Chem. Res.* **2014**, 53, 12363.

[16] Z.H. Dong, T. Liu, H.F. Liu, *Biofouling* **2011**, 27, 487.

[17] C. Sun, J. Xu, F. Wang, *Ind. Eng. Chem. Res.* **2011**, 50, 12797.

[18] H. Liu, D. Xu, A.Q. Dao, G. Zhang, Y. Lv, H. Liu, *Corros. Sci.* **2015**, 101, 84.

[19] H. Allwright, H. Enshaei, *Journal of Basic and Applied Scientific Research* **2016**, 6, 28.

[20] J. Landoulsi, K.E. Cooksey, V. Dupres, *Biofouling* **2011**, 27, 1105.

[21] X. He, P. Cao, F. Tian, X. Bai, C. Yuan, *Surf. Coat. Technol.* **2019**, 358, 159.

[22] F. Guan, X. Zhai, J. Duan, J. Zhang, K. Li, B. Hou, *Surf. Coat. Technol.* **2017**, 316, 171.

[23] X. He, P. Cao, F. Tian, X. Bai, C. Yuan, *Surf. Coat. Technol.* **2019**, 357, 180.

[24] Y. Hua, R. Barker, A. Neville, *J. Supercrit. Fluid.* **2015**, 97, 224.

[25] Y. Hua, R. Barker, A. Neville, *Corrosion* **2015**, 71, 667.

[26] I. Lanneluc, M. Langumier, R. Sabot, M. Jeannin, P. Refait, S. Sablé, *Int. Biodeter. Biodegr.* **2015**, 99, 55.

[27] C. Ruby, M. Abdelmoula, S. Naille, A. Renard, V. Khare, G. Ona-Nguema, G. Morin, J.-M.R. Génin, *Geochim. Cosmochim. Ac* **2010**, 74, 953.

[28] H. Tanaka, R. Mishima, N. Hatanaka, T. Ishikawa, T. Nakayama, *Corros. Sci.* **2014**, 78, 384.

[29] R.A. De Motte, R. Barker, D. Burkle, S.M. Vargas, A. Neville, *Mater. Chem. Phys.* **2018**, 216, 102.

[30] M.I. Khan, T. Yasmin, *J. Fail. Anal. Prev.* **2014**, 14, 537.

[31] Y. Hua, R. Barker, T. Charpentier, M. Ward, A. Neville, *J. Supercrit. Fluid.* **2015**, 98, 183.

[32] R. Stadler, L. Wei, W. Fürbeth, M. Grooters, A. Kuklinski, *Mater. Corros.* **2010**, 61, 1008.

**SUPPORTING INFORMATION**

Additional supporting information is available in the online version of this article at the publisher's website or from the author.

Table S1: Fitting results of specimens under different situations

Figure S1: Corrosion morphology of the steel surface after 1 day, 3 days and 5 days immersion in ASW (a) and *P. tricornutum* suspension under light-dark cycle (b), 24 h-constant light cycle (c) and 24 h-constant dark cycle (d).

Figure S2: SEM of corrosion products and biofilm formation on samples after 1 day, 3 days and 5 days immersion in ASW (a) and *P. tricornutum* suspension under light-dark cycle (b), 24 h-constant light cycle (c) and 24 h-constant dark cycle (d). *P. tricornutum* adhered on the samples after 1 day immersion are highlighted by the blue circles.

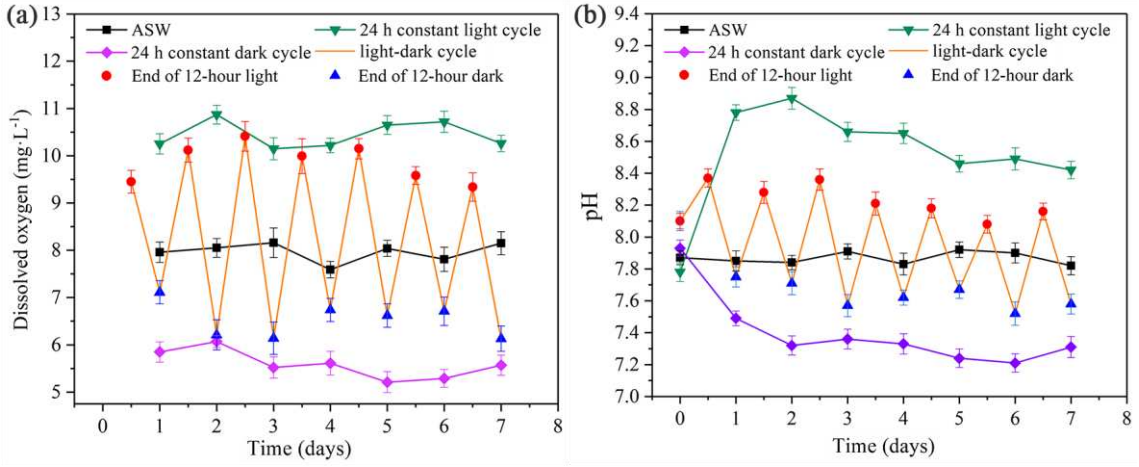


**Figure 1.** Concentration of dissolved oxygen (a) and recorded pH values (b) in ASW and *P. tricornutum* suspension under light-dark cycle, 24 h-constant light cycle and 24 h-constant dark cycle.

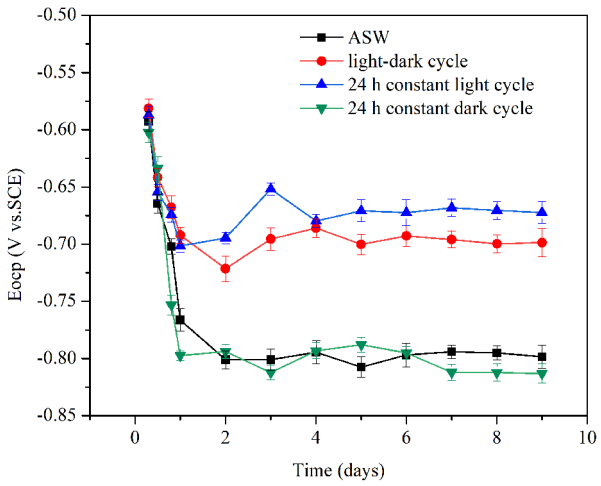


**Figure 2.** Open circuit potential curves of samples immersion in the ASW/*P. tricornutum* suspension at various cycles for 7 days.

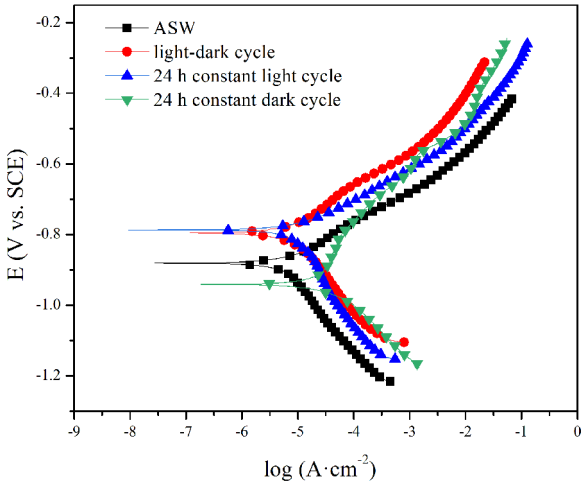


**Figure 3.** Polarization curves of samples after 7 days immersion in ASW/*P. tricornutum* suspension under light-dark cycle, 24 h-constant light cycle and 24 h-constant dark cycle.

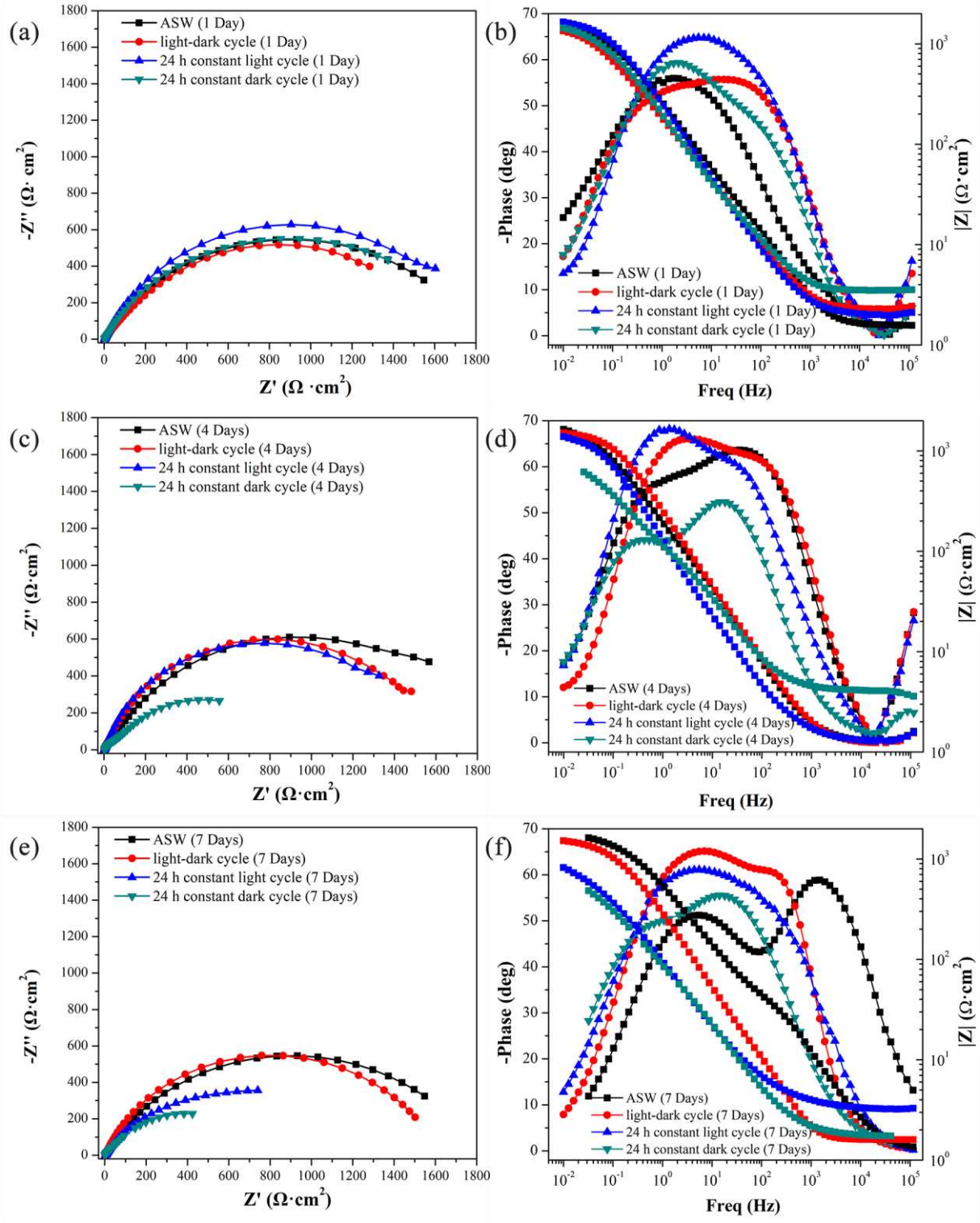


**Figure 4.** Nyquist plots (a, c, and e) and corresponding Bode plots (b, d, and f) under different cycles by the end of 1st, 4th and 7th day of exposure.

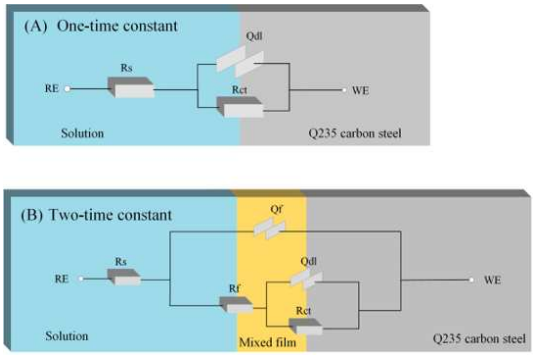


**Figure 5.** The equivalent circuits used to fit the EIS data.

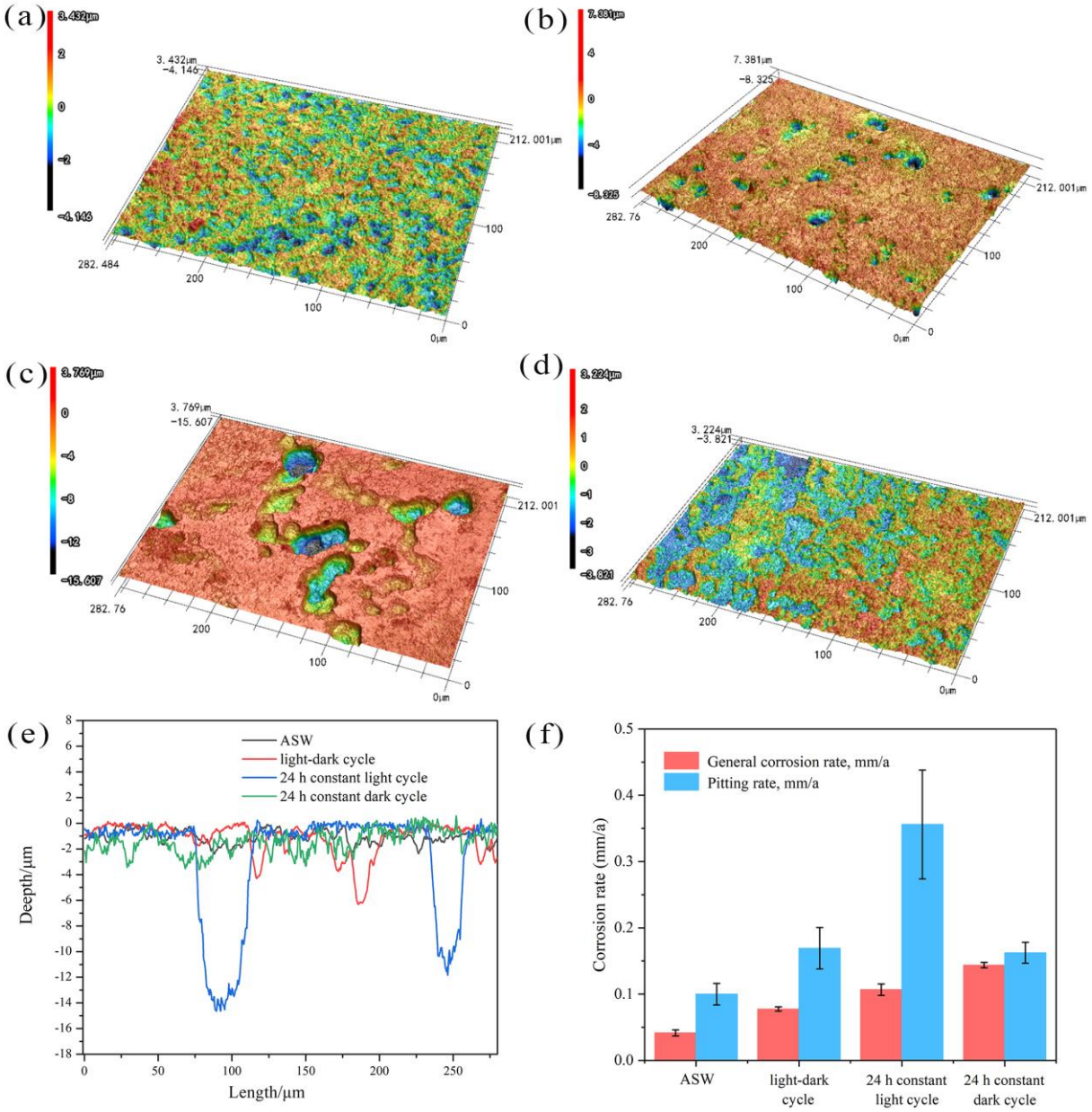

**Figure 6.** Corrosion morphology of the steel surface immersed in the ASW (a) and *P. tricornutum suspension* under light-dark cycle (b), 24 h-constant light cycle (c) and 24 h-constant dark cycle (d). The measured pit depths (e) and the calculated general corrosion rate and pitting rate (f). The total exposure time is 7 days.

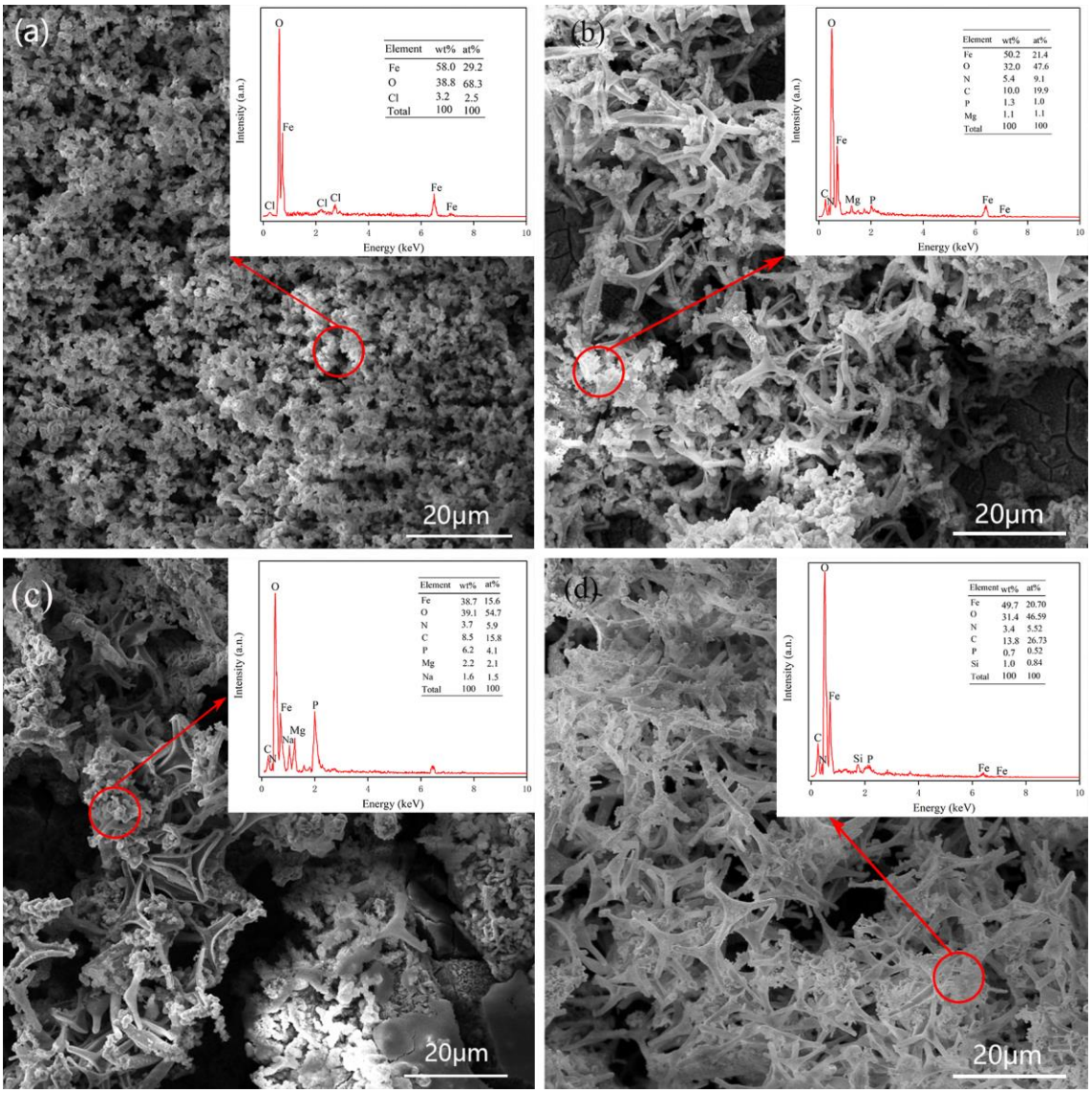


**Figure 7.** SEM and corresponding EDS results of the corrosion products and biofilm on sample surface after 7 days immersion in ASW (a) and *P. tricornutum* suspension under light-dark cycle (b), 24 h-constant light cycle (c) and 24 h-constant dark cycle (d).

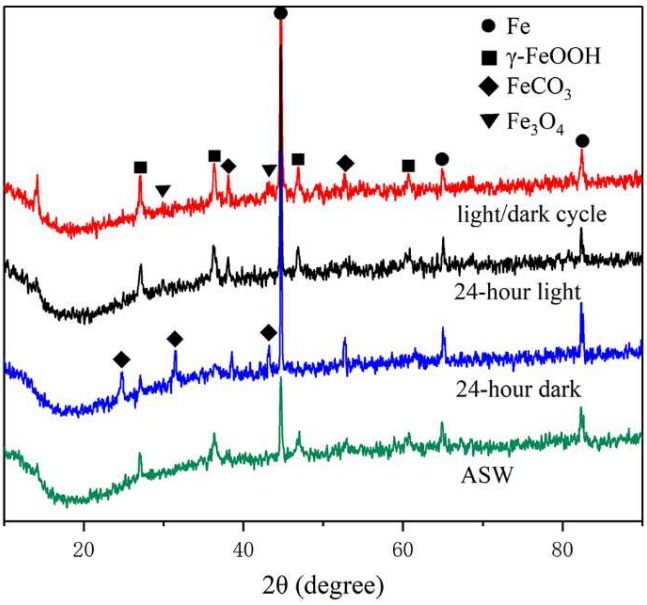


**Figure 8.** XRD patterns of the corrosion products after 7 days immersion in ASW and *P. tricornutum* suspension under various cycle conditions.

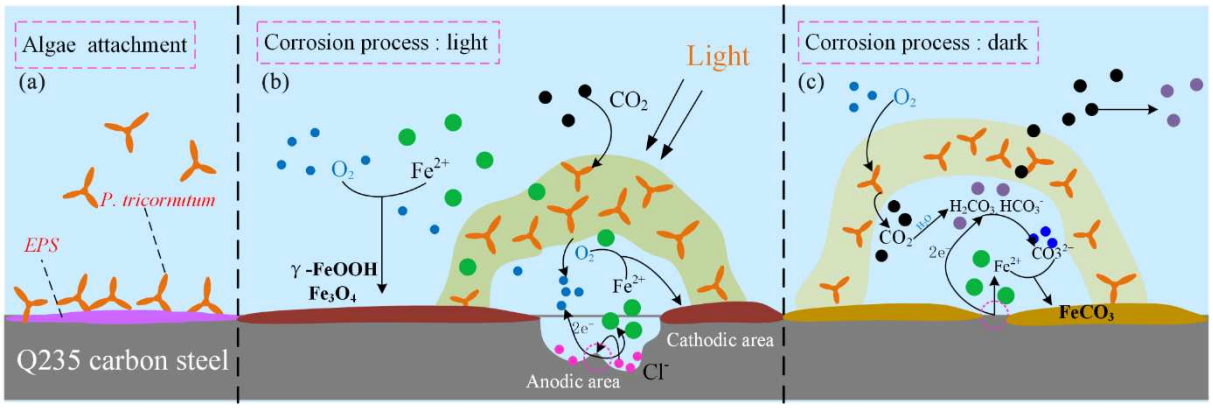


**Figure 9.** Attachment of *P. tricornutum* (a) and proposed corrosion mechanism of Q235 with the presence of *P. tricornutum* in light (b) and in dark (c).

**Table 1.** The experimental conditions

| | Solution | Conditions, cycles | Temperature | Immersion time (days) |
|---|---|---|---|---|
| Control group | ASW | / | 20 ± 0.1 ℃ | 1/2/3/4/5/6/7 |
| Experiment groups | P. tricornutum suspension | light-dark | | |
| | | 24 h-constant light | | |
| | | 24 h-constant dark | | |

**Table 2.** Electrochemical parameters fitted from the polarization curves after immersion for 7 days

| situation | Ba (mV) | Bc (mV) | Icorr ($10^{-6}$Amp·cm$^{-2}$) | Ecorr (V) | Corrosion rate (mm·a$^{-1}$) |
|---|---|---|---|---|---|
| ASW | 138.05±5.25 | 478.05±11.24 | 8.15±0.20 | -0.88±0.031 | 0.09±0.008 |
| Light-dark cycle | 152.26±8.32 | 267.26±8.75 | 12.31±0.58 | -0.78±0.035 | 0.14±0.009 |
| 24 h-constant light cycle | 170.09±6.79 | 382.80±11.21 | 17.26±0.91 | -0.79±0.043 | 0.21±0.011 |
| 24 h-constant dark cycle | 189.57±10.48 | 68.846±2.01 | 22.10±0.84 | -0.94±0.019 | 0.26±0.008 |

**Graphical Abstract**

The current study focuses on the *P. tricornutum* that influence the general and localized corrosion of carbon steel by a combination of immersion tests and electrochemical experiments. Photosynthesis of *P. tricornutum* increase the local oxygen concentration to inducing pitting corrosion. $CO_2$ produced by aspiration enhances the formation of crystalline $FeCO_3$ on the surface which provide better corrosion protection to the surface compare with γ-FeOOH and $Fe_3O_4$.

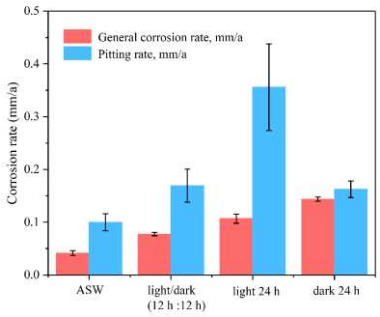


ToC figure